





Article

Ball-on-Disk Wear Maps for Bearing Steel–Hard Anodized EN AW-6082 Aluminum Alloy Tribocouple in Dry Sliding Conditions

Enrico Baroni ^{*}, Annalisa Fortini , Lorenzo Meo , Chiara Soffritti, Mattia Merlin  and Gian Luca Garagnani 

Department of Engineering (DE), University of Ferrara, Via G. Saragat 1, 44121 Ferrara, Italy; annalisa.fortini@unife.it (A.F.); lorenzo.meo@edu.unife.it (L.M.); chiara.soffritti@unife.it (C.S.); mattia.merlin@unife.it (M.M.); gian.luca.garagnani@unife.it (G.L.G.)

* Correspondence: enrico.baroni@unife.it

Abstract: In recent years, Golden Hard Anodizing (G.H.A.[®]) has been developed as a variant of the traditional hard anodizing process with the addition of Ag⁺ ions in the nanoporous structure. The tribological properties of this innovative surface treatment are still not well understood. In this study, ball-on-disk tests were conducted in dry sliding conditions using 100Cr6 (AISI 52100) bearing steel balls as a counterbody and GHA[®]-anodized EN AW-6082 aluminum alloy disks. The novelty of this work lies in the mapping of the wear properties of the tribocouple under different test conditions for a better comparison of the results. Three different normal loads (equal to 5, 10, and 15 N) and three different reciprocating frequencies (equal to 2, 3, and 4 Hz) were selected to investigate a spectrum of operating conditions for polished and unpolished G.H.A.[®]-anodized EN AW-6082 aluminum alloy. Quantitative wear maps were built based on the resulting wear rate values to define the critical operating limits of the considered tribocouple. The results suggest that the coefficient of friction (COF) was independent of test conditions, while different wear maps were found for polished and non-polished surfaces. Polishing before anodizing permitted the acquisition of lower wear for the anodized disks and the steel balls.

Keywords: aluminum alloy; hard anodizing; wear maps; ball-on-disk; dry sliding



Citation: Baroni, E.; Fortini, A.; Meo, L.; Soffritti, C.; Merlin, M.; Garagnani, G.L. Ball-on-Disk Wear Maps for Bearing Steel–Hard Anodized EN AW-6082 Aluminum Alloy Tribocouple in Dry Sliding Conditions. *Coatings* **2024**, *14*, 1469. <https://doi.org/10.3390/coatings14111469>

Academic Editor: Saideep Muskeri

Received: 20 October 2024

Revised: 13 November 2024

Accepted: 18 November 2024

Published: 19 November 2024



Copyright: © 2024 by the authors. Licensee MDPI, Basel, Switzerland. This article is an open access article distributed under the terms and conditions of the Creative Commons Attribution (CC BY) license (<https://creativecommons.org/licenses/by/4.0/>).

1. Introduction

Friction and wear occurring between mating and sliding surfaces are complex processes influenced by conditions and parameters ascribed to the tribological system [1,2]. Every damage process is determined by parameters such as loading conditions, characteristics of the two counterparts, and the interfacial elements between the two counterparts (i.e., lubricants, wear particles, abrasives, etc.) [3].

Despite this, most of the literature deals with the tribological characterization evaluating the effect of a single influencing factor. In order to facilitate a more expansive interpretation of the wear behavior of tribosystems, the utilization of wear maps represents an efficacious methodology for the visualization of tribosystem wear behavior, enabling the evaluation of the impact of at least two operating conditions. Wear maps are classification systems illustrating wear damage as a function of the various influencing factors understood as independent complex variables that can change continuously or in a discrete way [4–7]. Among the continuously variable factors, the most important are loading force, sliding speed, temperature, and time. The resulting material behavior map can be used as material and design selection guides to better understand the mechanisms that control wear [8]. Once the operating conditions to be investigated are fixed, the most representative contact geometry and friction mode are chosen according to one of the standard test methods [7]. The ball-on-disk test is widely applied in preliminary screen tests on materials for industrial applications, despite variations in surface geometry as sliding occurs, changing

the non-conformal contact to a conformal one [9]. Strict stationary conditions cannot be established as the contact pressure drastically evolves during contact, together with surface topography and the worn area [10].

Wear rate mapping in relation to test parameters can be considered as the first attempt at wear maps, and initially regarded for steel and cast irons in dry sliding conditions, to obtain three-dimensional quantitative wear maps. Wear mechanism maps were subsequently developed to deepen the wear characterization, providing information about the main ongoing wear mechanisms and transitions between different wear regimes [4,11]. Over the years, research on wear maps involving ferrous alloys has focused on the rail–wheel system, with the aim of enabling the selection of appropriate materials based on sliding speed and applied load (i.e., contact pressure) [2,12–14].

The development of wear maps for ceramic materials resulted from the increased reliability of their application in tribological contacts and was initially applied to the most used alumina, silicon nitride, zirconia, and silicon carbide [7,15–18]. Due to the growing practical relevance of ceramic coatings, their wear mapping is still a discussed topic in the literature [5,7].

Among the different functional coatings and means of metallic surface processing, anodizing treatments enable the growth of an anodic oxide layer that improves the hardness and wear resistance of aluminum (Al) alloys [19,20]. The growth of a compact Al oxide, consisting of a very thin and pore-free layer (the so-called barrier layer) and a thicker overlying nano-porous layer, is promoted by immersing the alloy in a sulfuric, phosphoric, oxalic, or chromic electrolytic solution. The overall thickness of the anodized layer can vary in the range of 10–20 μm for conventional anodizing processes, and up to 150 μm in the case of hard anodizing processes, which can be obtained by suppressing the dissolution process, typically decreasing the bath temperature [21]. The resulting hard anodized Al oxide layer ensures a better wear resistance than conventionally anodized Al alloys [22].

A relevant number of scientific papers investigating the tribological properties of different Al alloys in sliding contact with Fe-based alloys [23–27] and ceramics [21,27–30], and considering a wide range of wear test parameters, can be found in the literature. It is known that anodic layers with satisfactory wear resistance are easy to achieve for Al–Mg–Si alloys, in addition to their good strength after precipitation hardening [28], but their wear resistance has been studied considering a selected alloy and testing different sliding conditions in terms of sliding speed and applied load.

The wear behavior of a hard anodized AA6082-T5 in sulfuric acid was studied in a block-on-ring tribometer by Sola et al. [31]. According to the ASTM G77 standard, a rotating 100Cr6 cylinder slid against the stationary anodized sample, generating a conformal contact. The sliding speed was set equal to 0.3 m/s and 5, 20, and 40 N were applied as normal loads. It was found that the coefficient of friction increased at 40 N, while it stayed constant and between 0.65 and 0.85 at 5 and 20 N. The wear depth gradually increased while increasing the applied load and reaching the coating failure. Wide microcracks and an iron-oxide based transfer layer were found within the wear track. The specific wear rate was not provided by the authors. The influence of anodizing parameters, such as the electrolytic bath composition, on the mechanical properties and the tribological behavior of a hard anodized 6061-T6 alloy was investigated by Mohitfar et al. [28]. Unidirectional ball-on-disk tests were conducted using an alumina sphere with a 6 mm diameter and applying a 10 N normal load. Among the anodizing process carried out in sulfuric acid solution, abrasion and micro-cutting were found as the main wear mechanisms, and a coefficient of friction between 0.58 and 0.82, depending on the anodizing conditions, was determined. The specific wear rate varied between 1.0×10^{-14} and 1.5×10^{-13} m^3/Nm among the different combinations of parameters.

The commercial hard anodizing process denoted as G.H.A.[®] (Golden Hard Anodizing) performed on an EN AW-6060 Al alloy was investigated by Soffritti et al. [26] and compared to a traditional hard anodic oxide layer. The tribological properties of the anodic layers were investigated considering three different thicknesses equal to 25, 50, and 100 μm for

each anodizing treatment considered. Disks made in 100Cr6 steel were selected as the counterbody in unidirectional wear tests under an applied load equal to 10 N, at a sliding speed of 0.1 m/s and a 250 m total sliding distance. The formation of well-adherent, compacted, and plate-shaped wear particles on the wear tracks was found to determine the wear behavior of the considered couplings. The average coefficient of friction ranged between 0.34 and 0.50 among all the considered anodized layers, while the specific wear rate varied in the range between 1.0 and $5.0 \times 10^{-5} \text{ mm}^3/\text{Nm}$. The authors found that the tribological behavior of the anodic layer could be improved by a sealing process in hot water. Santecchia et al. [27] focused on the same commercial coating coupled both with 100Cr6 and Si_3N_4 balls by considering EN AW-6082 Al alloy as the substrate. Unidirectional tests were conducted at a 0.1 m/s sliding speed and applying a 5 N load until a 250 m sliding distance was reached. Three different anodic oxide layers differing in the resulting thickness (10, 50, and 100 μm , respectively) were considered to evaluate the tribological behavior. An iron oxide-based tribolayer was found when the 100Cr6 was considered as the counterbody material, determining a 0.8 coefficient of friction. It increased up to 0.9 when Si_3N_4 was used as the counterbody material, which was determined through failure and delamination of the anodic layer. The different wear mechanisms led to different specific wear rate values, between 3 and $4 \times 10^{-5} \text{ mm}^3/\text{Nm}$ for G.H.A.[®]/100Cr6 tribocouple and between 6 and $9 \times 10^{-5} \text{ mm}^3/\text{Nm}$ for G.H.A.[®]/ Si_3N_4 tribocouple.

However, to the best of the authors' knowledge, no works were found addressing the wear mapping of hard anodized Al alloys in sliding conditions against any of the most studied counterbody materials. This lack of knowledge makes any comparison with currently available data challenging. In light of this, the present paper deals with the elaboration of quantitative wear maps for an EN AW-6082 aluminum alloy treated following the innovative G.H.A.[®] anodizing process coupled with 100Cr6 steel balls in reciprocating wear tests. A set of wear test parameters, considering three different normal loads and three different reciprocating frequencies, was considered to investigate the wear behavior of the adopted tribocouple. The effect of a previous superficial polishing procedure was also taken into account to evaluate its influence on the morphological, mechanical, and tribological properties of the anodized layers. Based on the results, quantitative wear maps were built through a tailored MATLAB[®] version R2023a script and provided both for polished and unpolished anodized samples, coupled with a qualitative evaluation of the wear tracks through scanning electron microscopy. Interrupted wear tests were performed to evaluate the evolution of the wear of the counterbodies during sliding.

2. Materials and Methods

Disks with a 75 mm diameter and a 3 mm thickness were made in commercially available EN AW-6082 Al alloy with a nominal chemical composition in agreement with the UNI EN 573-3:2022 standard. Half of the disks underwent an industrial polishing procedure, whose details are confidential, to reduce the initial surface roughness. The remaining part was not subject to any polishing. These conditions are referred to as P (polished) and UP (unpolished) hereafter. All the disks were subsequently hard anodized according to the innovative G.H.A.[®] process. The latter was carried out in a sulfuric acid bath, following a galvanostatic process at a constant current density and temperature ranging between 1 and 10 A/dm² and 0 and 1 °C, respectively [32]. The resulting anodic oxide layers were then sealed in boiling water (100 °C) at a sealing rate of 2 min/ μm . Polished and unpolished samples were labeled as P and UP, respectively. Designation of the innovative hard anodizing treatments considered in this work, together with a summary of the related sealing parameters and eventual industrial polishing, are reported in Table 1.

Roughness parameters (R_a , R_q , and R_z) were measured using a Talysurf CCI Lite non-contact 3D profilometer (Taylor-Hobson, Leicester, UK) to evaluate the surface morphology of polished and unpolished samples. Five measurements were performed on each anodized surface and the average value together with its standard deviation were calculated for each parameter.

Disks were sectioned to obtain representative cross-sections, oriented perpendicularly to the coating surface. These sections were embedded in epoxy resin and subjected to standard metallographic preparation consisting of grinding with SiC abrasive papers ranging from 120 to 1200 grit, followed by polishing with diamond water-based suspensions. The average thickness of the anodized layers was measured using a Leica DMI8 A optical microscope (Leica, Wetzlar, Germany). For each anodized sample, at least five thickness measurements were taken from five distinct micrographs.

Microhardness was evaluated on the cross-section of the different samples by a Vickers Future-Tech FM-110 (Future-Tech Corp., Kawasaki, Japan) hardness tester. A load of 10 gf was applied for a 15 s dwelling time. Results are expressed as the mean of at least ten measurements on each oxide layer and provided with their respective standard deviation.

Reciprocating tribological tests were conducted in ball-on-disk configuration using a TR-20LE (Ducom Instruments, Bengaluru, India) tribometer in dry sliding conditions. Balls of 100Cr6 steel with a 10 mm diameter were selected as counterbodies. Temperature (25 °C) and relative humidity (40%–50%) of the room were considered as the environmental conditions during testing. The coefficient of friction (COF) and the system wear were continuously monitored by the instruments during wear tests. A maximum sliding distance equal to 200 m and a 25 mm stroke length were selected based on previous work by the authors to guarantee the assessment of a steady-state wear regime [26]. Three different normal load values (5, 10, and 15 N) and three different reciprocating frequencies (2, 3, and 4 Hz) were varied to evaluate their effect on the COF and the wear of the two counterbodies. Additionally, interrupted tests were conducted to evaluate the evolution of the wear of the two counterbodies over the sliding distance. Distances of 50, 100, and 150 meters were selected as monitoring intervals to assess wear evolution. For the sake of clarity, tests with 50, 100, and 150 m sliding distances were performed in triplicate, while five tests were conducted for 200 m as the sliding distance.

The hertzian contact pressure was calculated according to Hertz theory for a sphere-on-plane contact at each interval based on the mechanical properties of the considered material collected in Table 1. The reduced equivalent elastic modulus of the anodized Al alloy was calculated according to the model proposed by Liu et al. [33]. This method was selected because of its intuitive nature and intrinsic possibility to generalize the properties of both the coating and the substrate, instead of solved analytic models and equations [34–36].

Table 1. Mechanical properties of the different materials involved in the hertzian contact under examination.

	Young Modulus [GPa]	Poisson's Ratio
100Cr6 (ball)	210 ¹	0.30 ¹
EN AW-6082 (disk/substrate)	69 ²	0.33 ²
Anodic oxide layer (disk/coating)	90 ³	0.24 ³

¹ According to Ortega-Alvaréz et al. [37]. ² Estimated from data sheets provided by the suppliers. ³ According to Tsyantsaru et al. [29].

The wear tracks on the disks were analyzed through the same Talysurf CCI Lite non-contact 3D profilometer (Taylor-Hobson). At least five measurements were performed along the track to calculate the volume of the worn material. The specific wear rate (WR) was then obtained as the ratio between the volume loss and the product of the sliding distance and the applied load [38]. The wear of the steel balls was evaluated through a Leica MZ6 (Leica, Wetzlar, Germany) stereomicroscope. The dimensions of the wear track on the spheres were measured and the worn material calculated following the ASTM G99 standard [39]. Tailored MATLAB[®] code was elaborated to develop the quantitative wear maps for both the counterparts to illustrate the wear rate as a function of sliding speed

and normal load. Zones of the map presenting the same color indicate a similar wear rate, corresponding to a specific value provided by the color bar.

Relative WR of the disks was calculated at the end of each investigated sliding distance interval to monitor the evolution of both counterbodies [40], according to the following equation:

$$WR_{i,i-1} = \frac{V_i - V_{i-1}}{P \cdot (L_i - L_{i-1})} \quad (1)$$

where $WR_{i,i-1}$ is the specific wear rate in the interval between L_i and L_{i-1} partial sliding distances, determined by the volume loss in the same distance interval and calculated as the difference between V_i (worn volume at the i distance) and V_{i-1} (worn volume at the $i-1$ distance); P is the applied normal load. The WR value should be interpreted according to Kato and Adachi [41], who suggested $10^{-6} \text{ mm}^3/(\text{Nm})$ as the value for the transition between mild and severe wear, generally occurring from 10^{-9} to 10^{-6} and from 10^{-6} to $10^{-2} \text{ mm}^3/(\text{Nm})$, respectively.

The morphological investigation of the wear tracks on the anodized disks was carried out through a ZEISS EVO MA 15 (Zeiss, Oberkochen, Germany) scanning electron microscope operating in variable pressure conditions and coupled with an Oxford X-Max 50 (Oxford Instruments, Abingdon-on-Thames, UK) microprobe for energy-dispersive spectroscopy (VPSEM/EDS).

3. Results and Discussion

Optical micrographs of the cross-section of the anodized layers before wear tests are reported in Figure 1. Both the barrier layer and nanoporous structure cannot be distinguished due to their very low thickness, as stated in the literature. According to the hard anodizing low electrolytic bath temperature, the anodized layers in both the UP and P conditions reached a slightly high thickness exceeding $55 \mu\text{m}$. The anodized layers presented microporosities associated with intermetallic particles trapped in the coating during its growth (see the green circles in the micrographic pictures reported in Figure 1a,b), similar to those observed by Soffritti et al. [26] in the G.H.A.[®]-anodized EN AW-6060 substrate. Cracks along the cross-section were detected on the anodic oxide layers (see the red arrow depicted in Figure 1a) and are attributable to the industrial sealing process which the disks underwent, according to the literature [42].

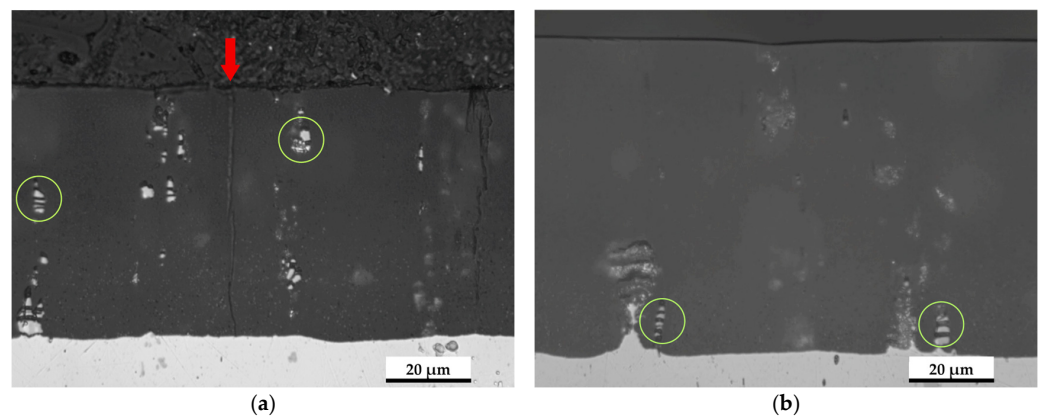


Figure 1. Optical micrographs in cross-section of the anodized layers before wear tests for (a) UP. (b) P.

The mean values of thickness, Vickers microhardness, and surface roughness parameters (R_a , R_q , R_z) of the anodized layers are collected in Table 2, together with their respective standard deviations. Both thickness and roughness were shown to be influenced by the polishing procedure, since P presented the highest thickness and the lowest R_a , R_q , and R_z roughness values. These experimental findings agree with the results of previous works in the literature [43,44]. Moreover, P showed a slightly higher average thickness than those

previously reported for G.H.A.[®] layers [26,27]. It appeared that Vickers microhardness was not influenced by the polishing procedure, with the two anodized layers showing similar values, which were higher than the substrate layer (115 ± 6 HV0.01).

Table 2. Thickness, Vickers microhardness (HV0.01), and roughness parameters (Ra, Rq, Rz) of the different anodized layers.

	Thickness [μm]	HV0.01	Ra [μm]	Rq [μm]	Rz [μm]
UP	57 ± 1	480 ± 17	1.01 ± 0.18	1.45 ± 0.30	14.61 ± 4.42
P	72 ± 1	482 ± 15	0.51 ± 0.01	0.65 ± 0.03	3.91 ± 0.39

The evolution of COF during sliding distance for UP and P samples is reported in Figure 2, collecting each investigated condition. As a general trend, it can be observed that the COF evolution and its average value remain constant regardless of the applied load. In fact, no direct correlation between the COF and the applied load was found. Moreover, the COF increased at the beginning of sliding but then remained almost constant until the end of the test. Based on this evidence, it can be assumed that the wear mechanisms governing the COF trend remained constant until the end of the test. When a 10 N load was applied (Figure 2b), it appeared the reciprocating frequency did not influence the COF, as the COF presented similar trends and average values in a small range of around 0.6. At a load equal to 15 N, the COF was lower in the case of the P anodized layer with respect to UP at each reciprocating frequency, but the same correlation did not occur at the lower loads. For the sake of clarity, fluctuations in the COF curves may also be associated with the recording features of the instrument, according to the intrinsic oscillatory nature of the reciprocating motion.

The mean values of steady-state COF of the tribocouple in the different tested conditions are collected in Table 3, together with their respective standard deviations. Based on the trends presented in Figure 2, the COF was considered to be steady after a sliding distance equal to 25 m. In light of this, the mean values and their standard deviations are calculated for all the tests performed at the same test parameters. As a general trend, it can be observed that the P sample showed higher COF values than the UP sample if the same testing parameters were considered. Since the hardness of UP and P anodic layers was 480 ± 17 and 482 ± 15 HV0.01, respectively, it can be assumed that the roughness of the two surfaces played a key role. The standard deviation for the same P samples was larger in each tested condition. Moreover, the most comparable COF values between UP and P samples were obtained under the effect of a 10 N load, regardless of the reciprocating frequency (i.e., of the average sliding speed). When the frequency was equal to 4 Hz, the lowest COF was obtained for both the anodized disks and all the applied loads.

The obtained COF values are similar to the ones reported by Sola et al. [31], but the same significant increments could not be found in the investigated load range.

Table 3. Mean values and related standard deviations of the steady-state coefficient of friction for all test conditions.

Disk		5 N	10 N	15 N
UP	2 Hz	0.55 ± 0.03	0.60 ± 0.02	0.61 ± 0.01
	3 Hz	0.60 ± 0.02	0.64 ± 0.03	0.55 ± 0.01
	4 Hz	0.56 ± 0.01	0.58 ± 0.02	0.52 ± 0.02
P	2 Hz	0.63 ± 0.04	0.60 ± 0.04	0.62 ± 0.05
	3 Hz	0.64 ± 0.03	0.62 ± 0.03	0.59 ± 0.04
	4 Hz	0.57 ± 0.03	0.62 ± 0.02	0.59 ± 0.02

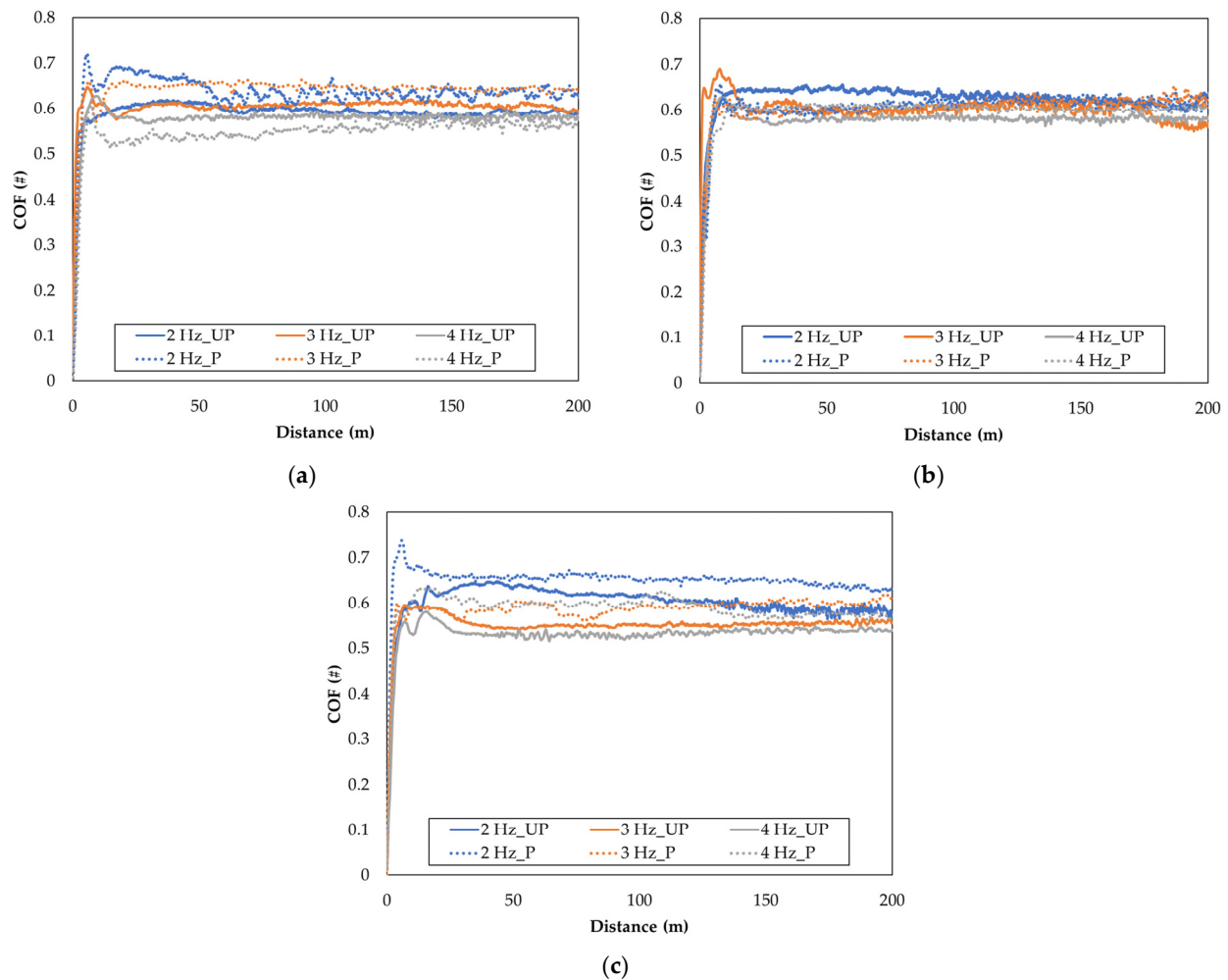


Figure 2. COF evolution during distance for UP (unpolished substrate) and P (previously polished substrate) anodic layers at the different investigated loads: (a) 5 N, (b) 10 N, and (c) 15 N.

To better understand the wear behavior of the G.H.A.[®] anodic layer coupled with 100Cr6 steel balls, the wear tracks were analyzed through electronic microscopy. Representative micrographic images are collected in Figure 3 at the different distance intervals considered in this study, i.e., 50, 100, 150, and 200 m. Firstly, it can be observed that the same general aspect of the wear track remains constant along the sliding distance, confirming the assumption made by discussing the variation in COF with sliding distance (see Figure 2). A white diffused tribolayer was observed after each interval, and its extension perpendicular to the sliding direction (orange arrow) indicates the growing width of the wear tracks. The tribolayer appeared to differ on each surface, probably due to its fragmentation by stress cycling and local detachment once a critical thickness was reached. These observations agree with those of other authors dealing with the same tribocouple [26,27,31]. A very similar behavior was observed by Malayoglu et al. [45], who studied the tribological behavior of hard anodized EN AW-6082 alloy against Si₃N₄ balls. The same wear mechanisms were observed, and the authors attributed the formation of the tribolayer to the asperities on the wear track.

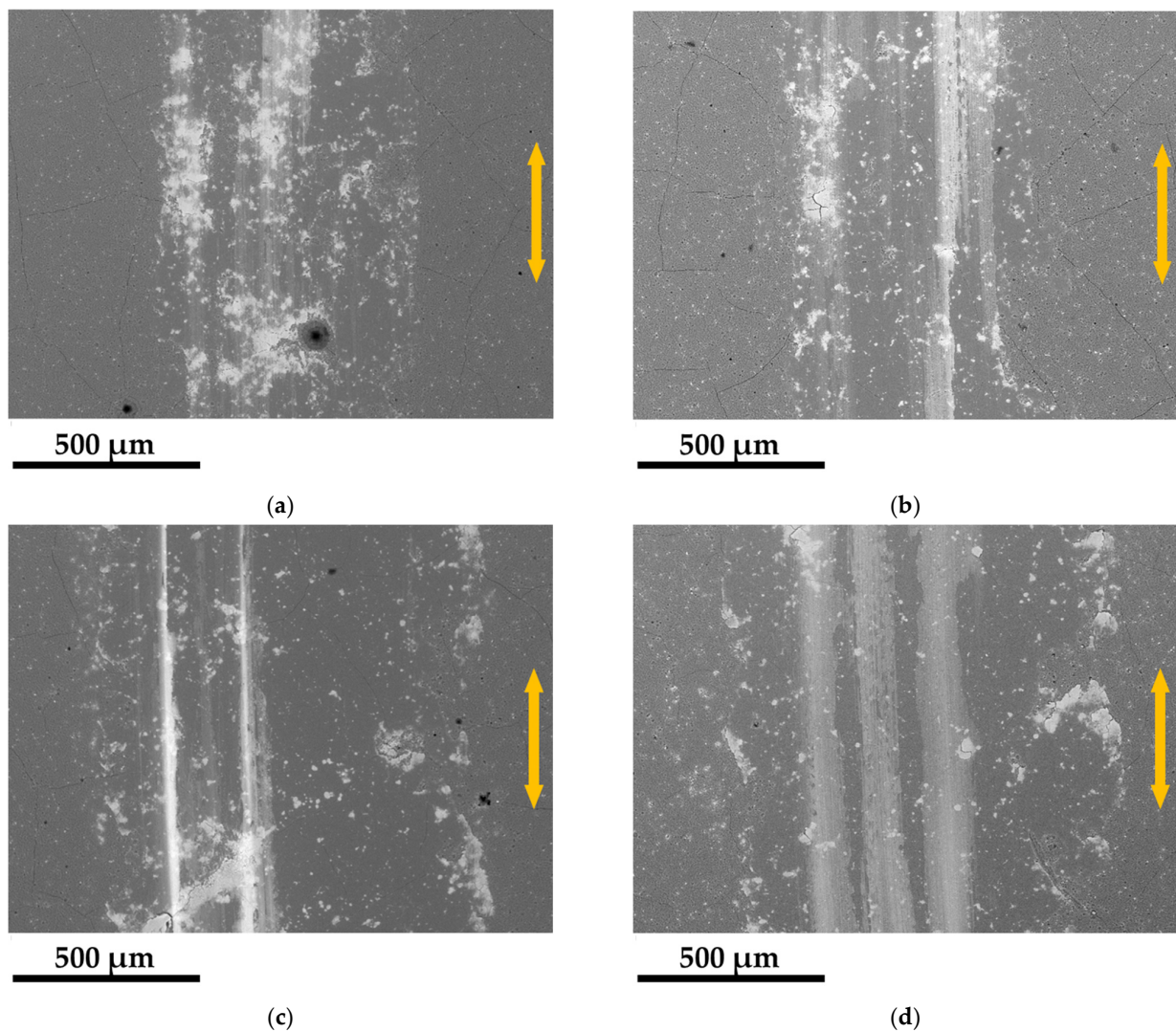


Figure 3. Representative VPSEM micrographs of wear tracks of the G.H.A.[®]-anodized disk (a) after 50 m, (b) after 100 m, (c) after 150 m, and (d) after 200 m. The orange arrow indicates the direction of reciprocating sliding.

Wide microcracks without any preferential direction can also be noticed as being uniformly distributed inside and outside the wear track. They can be attributed to the shear stresses during sliding contact, which could exceed the deformation ability of the anodized layers. On the other hand, the same kind of microcracks could be attributed to the heat of the sealing process of the anodic layer, as pointed out by Liu et al. [46].

Figure 4 shows a VPSEM micrograph at a higher magnification of the center of the wear track together with two semi-quantitative EDS spectra. A compacted and well-adherent tribolayer can be observed on the wear track, showing cracks and detachment areas (see the solid red arrow in Figure 4a). Regarding the semi-quantitative EDS spectrum acquired in the zone pointed out by the solid red arrow and reported in Figure 4b, a high amount of oxygen (O) was revealed together with high contents of iron (Fe) and Al, suggesting that the tribolayer may be formed by iron oxide and anodic oxide detached particles. High amounts of O, Al, and Ag were revealed through semi-quantitative EDS analyses in the pits generated by the detachment of the tribolayer and part of the anodic oxide layer (see the yellow-edged arrow and its respective EDS spectrum in Figure 4c). Finally, the red-edged arrow indicates the deposition of a newer tribolayer, which appears in a light grey because of its reduced thickness.

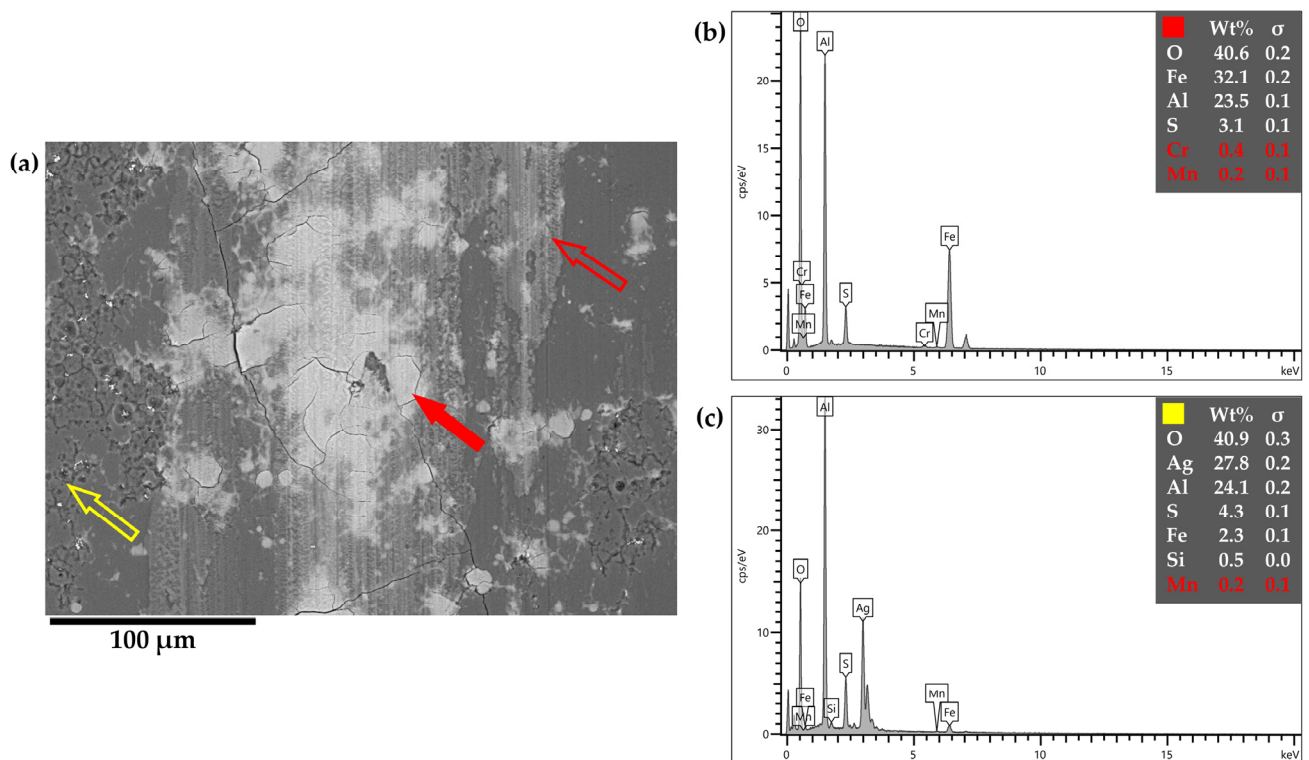


Figure 4. VPSEM micrograph at high magnification of the wear tracks of the disk together with semi-quantitative EDS spectra (a). The solid red arrow indicates the area of revelation for the semi-quantitative EDS analysis (b). The red-edged arrow indicates the new deposition of material, while the yellow-edged arrow indicates the removal of a part of the anodic layer with its corresponding EDS spectra (c).

The contact pressure between the two counterparts was calculated at each interval to evaluate changes in contact dynamics. Figure 5 shows the hertzian contact pressures against the sliding distance, for each applied load considering P disks as the representative case. Before sliding, the contact pressure was high due to the sphere-on-plane geometry following Hertz's theory (the hertzian contact pressure varied between 351 in the case of 5 N and 506 MPa in the case of 15 N, while the contact diameter varied in the range between 135 and 195 μm , depending on the considered load). Once the sliding between the two counterbodies is initiated, their surface morphology changes because of wear phenomena, and the contact geometry needs to be checked and recomputed. It was found that after 50 m of sliding, the average scar diameter on the 100Cr6 exceeded 500 μm in all the considered sets of test parameters. Ravikiran et al. [40] suggested that when the area of the wear scar exceeds the initial hertzian contact area, the contact pressure can be calculated as hydrostatic pressure and contact can be considered as conformal. Based on this, the order of magnitude of the applied pressure is lower and almost constant through the other sliding distance intervals.

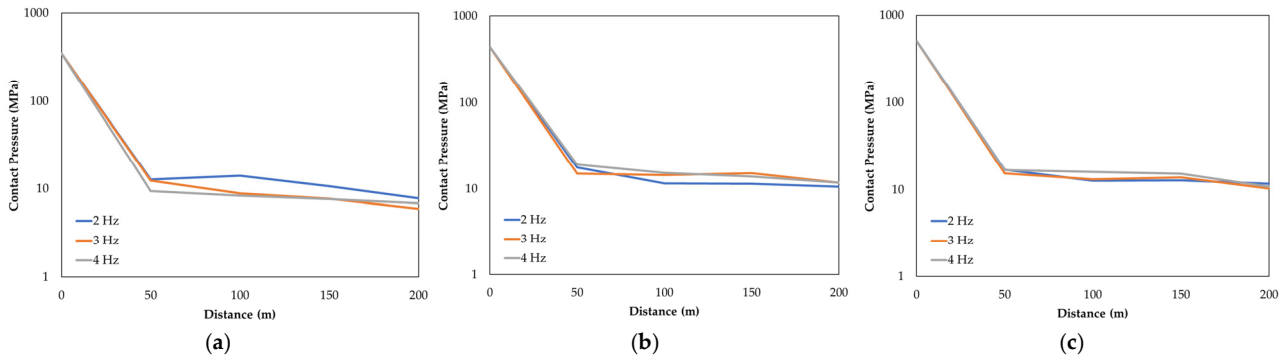


Figure 5. Contact pressure evolution during sliding distance for the different applied loads: (a) 5 N, (b) 10 N, and (c) 15 N. Y-axis is reported in logarithmic scale.

The worn volume from anodized disks and 100Cr6 balls was determined through optical 3D profilometry and stereomicroscopy analyses. The evolution of the worn material during the sliding distance for UP disks and 100Cr6 balls is reported in Figure 6, together with a shape factor of the wear scars on 100Cr6 steel balls (the so-called Wear Scar Diameter Variance), expressed as a percentage of the difference between the two measured perpendicular diameters. A difference of 5% was selected as a threshold for considering a wear scar as circular-shaped. The slope of each line linking two consecutive measured worn volumes gives information about the wear phenomenon: the counterpart was getting worn when the slope was positive (i.e., the worn volume grows in two consecutive fixed sliding distances reached), whereas material deposition was occurring when the slope was negative (i.e., the counterpart was gaining material from the counterpart). Regarding the wear scar diameter variance, it should be clear that a difference between the two main diameters $\geq 5\%$ should be considered as an indication of the ellipticity of the wear scar and consequent conformity of the contact between surfaces.

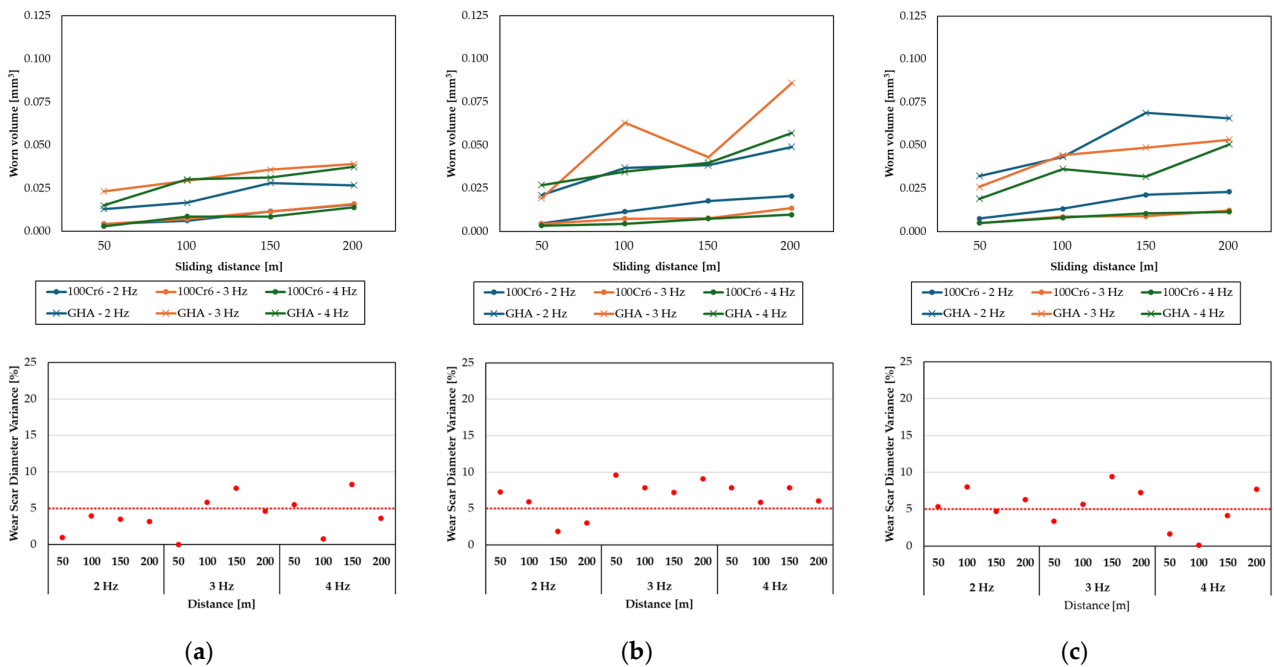


Figure 6. Worn volume of material from both the counterbodies at the different investigated loads in the case of sliding against UP samples together with a shape factor for the wear scar diameters on the 100Cr6 steel balls at (a) 5 N, (b) 10 N, and (c) 15 N.

As a general trend, it can be noticed that the wear of the counterbodies increased as the load increased, as the lowest worn material amount was found when the applied load

was 5 N (see Figure 6a). After a steep increase in the first 50 m interval, the worn volume for both disks and balls was found to grow smoothly (in each sliding distance interval the relative $WR_{i,i-1}$ ranged between -5.8×10^{-6} and $9.3 \times 10^{-5} \text{ mm}^3/(\text{Nm})$ for the disks and around $2.2 \times 10^{-5} \text{ mm}^3/(\text{Nm})$ for the balls). Looking at the corresponding wear scar diameter variance graph, it can be observed that at each investigated test condition, the diameters appeared quite similar, confirming the near-mild ongoing wear regime. It was found that, at 5 N, the lowest frequency of 2 Hz permitted the minimization of wear of both disks and balls.

When increasing the load (see Figure 6b,c), the worn material amount growth rate (i.e., the wear rate or rate of wear) appeared steepest in most of the intervals, while the slope of each interval was found to be alternatively positive and negative, suggesting material deposition and removal as alternate phases of the wear mechanism, confirming the VPSEM wear track morphology observation. The shape of the wear scars on the 100Cr6 steel balls was found to be elliptical (variance $\geq 5\%$) at most of the sliding distance intervals, regardless of the load and the reciprocating frequency. This indicates a higher system wear and an assessed conformal contact between surfaces.

In Figure 7, the quantitative wear maps for the UP sample are reported, both for the 100Cr6 steel ball counterpart and the anodized layer itself. The WR values are reported as a function of reciprocating frequency and normal load. As a general trend, it can be stated that the WR decreased while the normal load for both the counterbodies increased. Moreover, the effect of the reciprocating frequency was clearly detectable considering the 100Cr6 steel: the lower the frequency, the higher the resulting WR. On the other hand, a clear trend was obtained for the UP anodic layer only at the lower load of 5 N. The lowest WR by the two counterbodies when a 15 N load was applied was detected, but different wear regimes were assessed: mild for the 100Cr6 steel (WR values ranging between 3.8 and $7.7 \times 10^{-6} \text{ mm}^3/(\text{Nm})$) at 10 and 15 N applied load, and severe for the 100Cr6 steel at 5 N (WR values ranging between 1.4 and $1.6 \times 10^{-5} \text{ mm}^3/(\text{Nm})$) and the anodic layer (WR ranging between 1.7 and $4.3 \times 10^{-5} \text{ mm}^3/(\text{Nm})$).

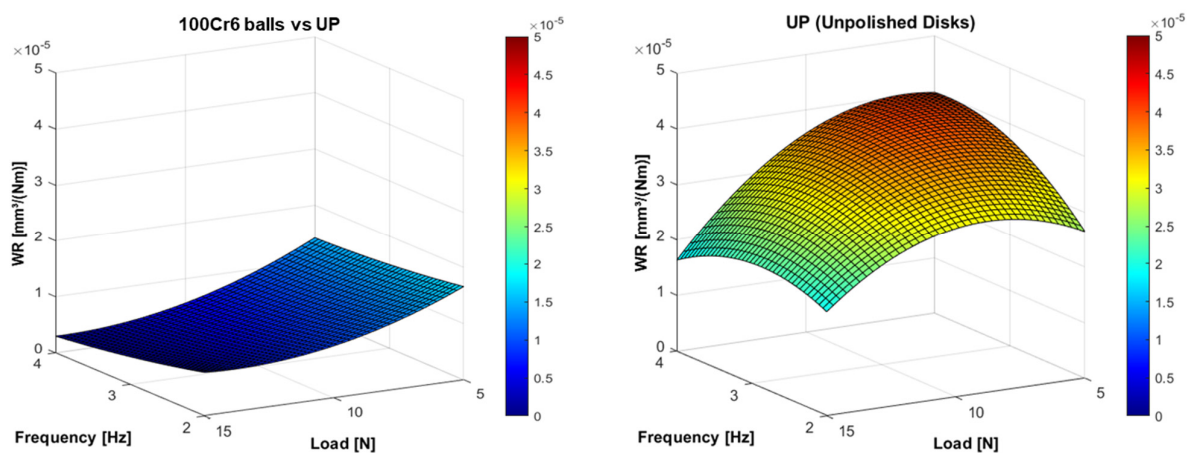


Figure 7. Quantitative wear maps for 100Cr6 ball and UP anodized disks.

At each load, the worn volume increased in each sliding distance interval, both for disks and balls. This could be related to the wear mechanism provided by the lowest roughness of the P anodic layer. As suggested in the literature, lower roughness can be attributable to a generally lower height of the asperities responsible for the tribolayer formation and compaction [45]. This could lead to a quicker delamination and particle detachment from the anodic layer, and the higher measured worn volume from the counterbodies could explain this phenomenon. At a 5 N applied load, the worn volume from the counterbodies was similar to those obtained on UP samples, with a negligible effect of the reciprocating frequency (see Figure 8a). The wear scar on the 100Cr6 was nearly elliptical, indicating the upcoming transition between non conformal and conformal contact. The worn volume of

material from both the P anodic layer and 100Cr6 steel was similar to the one measured at 5 N, except for the lowest reciprocating frequency, in which a huge transition after 150 m was detected: $WR_{100,50}$ and $WR_{150,100}$ were 3.8×10^{-5} and $2.2 \times 10^{-5} \text{ mm}^3/(\text{Nm})$, respectively, while $WR_{200,150}$ was found to be equal to $-7.3 \times 10^{-5} \text{ mm}^3/(\text{Nm})$, indicating material deposition from the ball to the disk. The highest worn volumes of material were obtained when 15 N was applied as the normal load. Concerning the worn volume from the P anodic layer, it was found to grow with a steep slope, showing the worst performance at 3 Hz and especially in the last 50 m of sliding (the $WR_{200,150}$ was equal to $5.89 \times 10^{-5} \text{ mm}^3/(\text{Nm})$). Conversely, the wear process of the 100Cr6 steel ball followed the same behavior at each reciprocating frequency. The dispersion of the wear scar diameter variance confirms that severe wear was ongoing at 15 N for each reciprocating frequency.

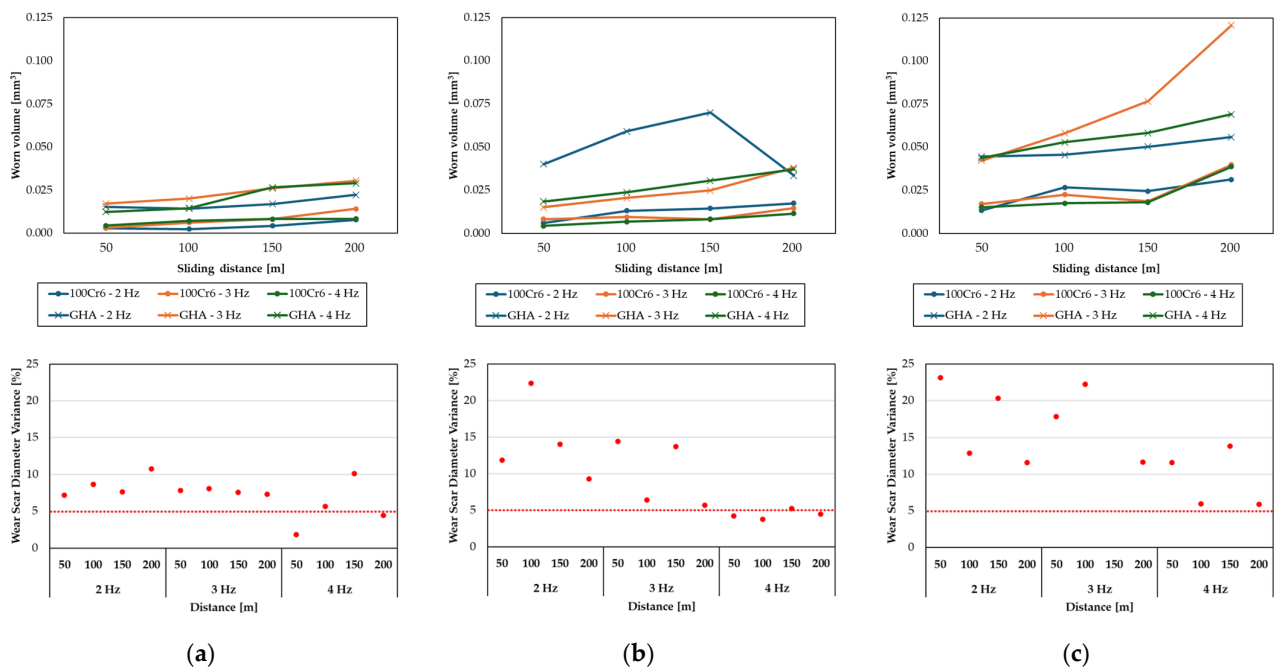


Figure 8. Worn volume of material from both the counterbodies at the different investigated loads in the case of sliding against P samples together with a shape factor for the wear scar diameters on the 100Cr6 steel balls at (a) 5 N, (b) 10 N, and (c) 15 N.

In Figure 9, the quantitative wear maps for the P sample are reported, both for the 100Cr6 steel ball counterpart and the anodized layer itself. The WR values are reported as a function of reciprocating frequency and normal load. 100Cr6 steel balls showed a near-mild wear regime when 5 and 10 N loads were applied (WR ranging between 5.7 and $8.4 \times 10^{-6} \text{ mm}^3/(\text{Nm})$). Under the action of the 15 N load, the severe wear regime was established, as suggested by the WR values in the range between 1.0 and $1.4 \times 10^{-5} \text{ mm}^3/(\text{Nm})$. The same variations among the test parameters were found for the wear of the P anodic layer. A severe wear regime was assessed at each investigated condition, as confirmed by the order of magnitude of the WR. The same macroscopic behavior was found at each load and 3 Hz resulted in the most impactful reciprocating frequency, determining WR values in the range of 1.9 and $4.0 \times 10^{-5} \text{ mm}^3/(\text{Nm})$.

For both UP and P disks, unexpected WR values were obtained at a 3 Hz frequency (i.e., a 0.15 m/s average sliding speed along the stroke length). A possible explanation could be found in the works dealing with the wear of ceramic materials, especially with alumina, as proposed by Ravikiran et al. [47,48]. The authors stated that critical sliding speed and load values, and the time interval between successive WR measurements, could be the causes of unexpected wear amounts, but further investigations should be performed

to assess the wear behavior on a broader range of operating conditions considering the stochastic nature of wear measurements [49].

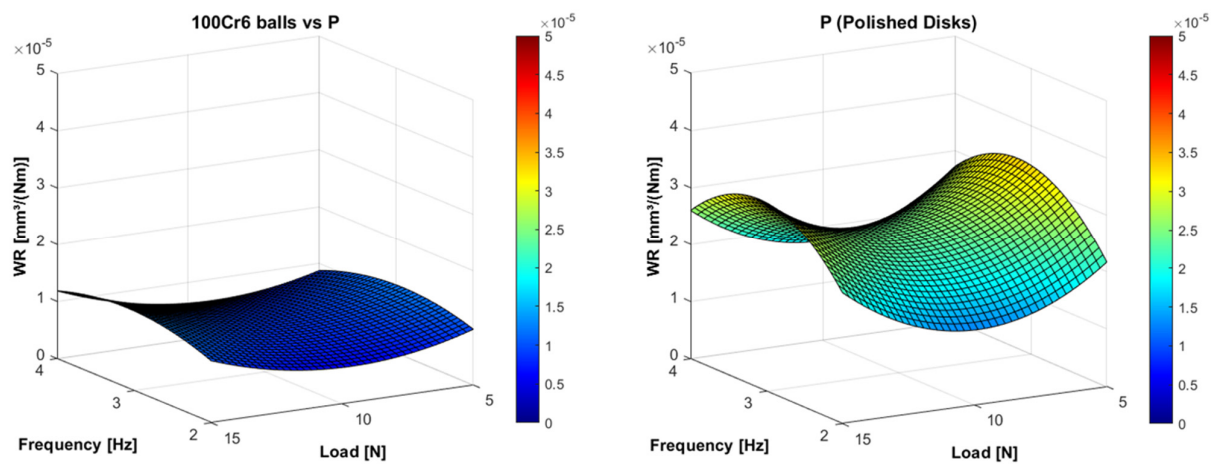


Figure 9. Quantitative wear maps for 100Cr6 ball and P anodized disks.

Comparing the quantitative wear maps, it can be assumed that both the anodic layers are worn quicker than the 100Cr6 steel counterpart, as demonstrated by the higher WR values at each considered test parameter combination. The polishing procedure affected the WR of the tribosystem, determining two different main behaviors. UP presented a reclined surface in which 5 N–4 Hz was the worst-case scenario (highest WR upon all the tested conditions), and the best tribological behavior was shown at 15 N and 2 Hz, minimizing the WR of both the 100Cr6 steel balls and the anodic layer. Conversely, P permitted the normalization of the WR for both 100Cr6 and the anodic layer, thereby reducing the impact of the test parameters on the resulting worn material.

4. Conclusions

In the present work, the tribological behavior of a G.H.A.[®]-anodized EN AW-6082 Al alloy was investigated with a spectrum of test parameters. Dry sliding reciprocating tests were conducted on the anodized layers obtained on Al alloy disks in two different surface preparations to deepen the effect of an industrial polishing procedure on the wear resistance of the coating. The three-dimensional wear maps for both the anodized layers and the 100Cr6 steel counterpart, together with the morphology of wear tracks evaluated through VPSEM analyses, permitted a better understanding of the wear behavior of the tribocouple in a determined range of operating parameters. Interrupted tests helped to clarify the progression and evolution phenomena of the wear of the two sliding counterparts.

Based on the obtained results, the following conclusions can be drawn:

- The preliminary industrial polishing procedure altered the morphological features of the anodic oxide layers. Polished disks (P) showed greater thickness and lower surface roughness (Ra, Rq, Rz) compared to unpolished disks (UP), but no difference in Vickers microhardness.
- The trend of the coefficient of friction (COF) for P/100Cr6 and UP/100Cr6 tribocouples was not affected by the applied load. However, P samples showed higher COF than UP samples sliding against 100Cr6 balls. The standard deviation for P samples was higher than that for the UP ones at the same investigated conditions. The lowest COF (0.52 ± 0.02) for both tribocouples occurred with 4 Hz and 15 N of applied load.
- UP disks exhibited the highest COF with 4 Hz and 5 N of applied load. The best tribological performance was seen at 15 N and 2 Hz, showing the lowest wear rate (WR) for both 100Cr6 steel balls and anodic layers. Conversely, P permitted the normalization of WR for both 100Cr6 and the anodic layer, thereby reducing the impact of the test parameters on the resulting worn material. For both UP and P disks,

unexpected WR values were obtained at a 3 Hz frequency (i.e., a 0.15 m/s average sliding speed among the stroke length) at each applied load.

- Interrupted tests revealed that the wear of the G/100Cr6 tribocouple is non-linear, especially at loads higher than 10 N, where transfer phenomena between counterbodies occur.

The results provided by the quantitative wear maps should be interpreted as a function of the selected boundary conditions, i.e., an anodic layer sliding against 100Cr6 steel (similar Vickers microhardness values, so the wear phenomena are quite unstable and involve both the counterbodies), reciprocating motion, medium-low frequency range (2–4 Hz), and medium-load range (5–15 N). As a future perspective, the wear mapping for the considered tribocouple could be expanded to lower normal loads (i.e., lower contact pressure) and a broader range of reciprocating frequencies to investigate the tribological properties and identify the operative conditions that minimize wear. Furthermore, the wear resistance of hard anodized Al alloy against a harder material could be evaluated in order to focus all the wear phenomena on the anodized layers.

Author Contributions: Conceptualization, E.B. and A.F.; methodology, E.B.; software, E.B. and L.M.; validation, A.F., C.S. and M.M.; formal analysis, A.F. and M.M.; investigation, E.B.; resources, A.F. and M.M.; data curation, E.B. and L.M.; writing—original draft preparation, E.B.; writing—review and editing, A.F., C.S. and M.M.; visualization, E.B. and A.F.; supervision, A.F. and G.L.G.; project administration, G.L.G.; funding acquisition, M.M. and G.L.G. All authors have read and agreed to the published version of the manuscript.

Funding: This research was funded by FAR 2024 funding from the University of Ferrara (Ferrara, Italy), aimed at the tribological characterization of wrought aluminum alloys treated by innovative hard anodizing treatments involving sealing of anodic oxide pores with silver ions.

Institutional Review Board Statement: Not applicable.

Informed Consent Statement: Not applicable.

Data Availability Statement: The raw data supporting the conclusions of this article will be made available by the authors on request.

Acknowledgments: The authors gratefully acknowledge G.H.A. Europe s.r.l. for supplying the materials and the anodizing treatments investigated in this work. The authors also wish to thank Franco Cicerchia, Costantino Cicerchia, and Alessandro Savelli for the technical assistance. The authors would also like to acknowledge Federico Faccin and Matilde Minotti for their cooperation in the tribological test campaign. A special thanks also to Mattia Piovan for the support in the graphical description of part of the data.

Conflicts of Interest: The authors declare no conflicts of interest.

References

1. Liu, Y.; Asthana, R.; Rohatgi, P. A Map for Wear Mechanisms in Aluminium Alloys. *J. Mater. Sci.* **1991**, *26*, 99–102. [[CrossRef](#)]
2. Zhang, B.; Ma, X.; Liu, L.; Yu, H.; Morina, A.; Lu, X. Study on the Sliding Wear Map of Cylinder Liner—Piston Ring Based on Various Operating Parameters. *Tribol. Int.* **2023**, *186*, 108632. [[CrossRef](#)]
3. Kato, K. Classification of Wear Mechanisms/Models. *Proc. Inst. Mech. Eng. Part J J. Eng. Tribol.* **2002**, *216*, 349–355. [[CrossRef](#)]
4. Lim, S.C.; Ashby, M.F.; Brunton, J.H. Wear-Rate Transitions and Their Relationship to Wear Mechanisms. *Acta Metall.* **1987**, *35*, 1343–1348. [[CrossRef](#)]
5. Lim, S.C. Recent Developments in Wear-Mechanism Maps. *Tribol. Int.* **1998**, *31*, 87–97. [[CrossRef](#)]
6. Hsu, S.M.; Shen, M. Wear Prediction of Ceramics. *Wear* **2004**, *256*, 867–878. [[CrossRef](#)]
7. Maros, M.B.; Németh, A.K. Wear Maps of HIP Sintered Si₃N₄/MLG Nanocomposites for Unlike Paired Tribosystems under Ball-on-Disc Dry Sliding Conditions. *J. Eur. Ceram. Soc.* **2017**, *37*, 4357–4369. [[CrossRef](#)]
8. Hsu, S.M. Wear Maps. In *Modern Tribology Handbook*; Bhushan, B., Ed.; CRC Press: Boca Raton, FL, USA, 2001; Volume 1.
9. Meozzi, M. Special Use of the Ball on Disc Standard Test. *Tribol. Int.* **2006**, *39*, 496–505. [[CrossRef](#)]
10. Kozyrev, Y.P.; Ginzburg, B.M.; Priemskii, N.D.; Tochilnikov, D.G.; Bulatov, V.P. Express Investigations of Wear Processes by Means of Cylindrical Counterbodies. Part I: Calculations and Technique. *Wear* **1994**, *171*, 71–75. [[CrossRef](#)]
11. Welsh, N.C. The Dry Wear of Steels I. The General Pattern of Behaviour. *Philos. Trans. R. Soc. Lond. Ser. A Math. Phys. Sci.* **1965**, *257*, 31–50. [[CrossRef](#)]
12. Lewis, R.; Olofsson, U. Mapping Rail Wear Regimes and Transitions. *Wear* **2004**, *257*, 721–729. [[CrossRef](#)]

13. Seo, J.-W.; Jun, H.-K.; Kwon, S.-J.; Lee, D.-H. Rolling Contact Fatigue and Wear of Two Different Rail Steels under Rolling–Sliding Contact. *Int. J. Fatigue* **2016**, *83*, 184–194. [[CrossRef](#)]
14. Vásquez-Chacón, I.A.; Gómez–Guarneros, M.A.; Sanchez-Tizapantzi, P.; Gallardo-Hernández, E.A. A Pin-on-Disk Wear Map of Rail and Wheel Materials from Different Standards. *Mater. Lett.* **2022**, *307*, 131021. [[CrossRef](#)]
15. Jahanmir, S. *Friction and Wear of Ceramics*; CRC Press: Boca Raton, FL, USA, 1993; ISBN 9780429181559.
16. Adachi, K.; Kato, K.; Chen, N. Wear Map of Ceramics. *Wear* **1997**, *203–204*, 291–301. [[CrossRef](#)]
17. Hsu, S.M.; Shen, M.C. Ceramic Wear Maps. *Wear* **1996**, *200*, 154–175. [[CrossRef](#)]
18. Hsu, S.; Lim, D.S.; Wang, Y.S.; Munro, R.G. Ceramics Wear Maps: Concept and Method Development. *Lubr. Eng.* **1991**, *47*, 49–54.
19. Lee, S.; Kim, D.; Kim, Y.; Jung, U.; Chung, W. Effect of Aluminum Anodizing in Phosphoric Acid Electrolyte on Adhesion Strength and Thermal Performance. *Met. Mater. Int.* **2016**, *22*, 20–25. [[CrossRef](#)]
20. Bensalah, W.; Elleuch, K.; Feki, M.; DePetris-Wery, M.; Ayedi, H.F. Comparative Study of Mechanical and Tribological Properties of Alumina Coatings Formed on Aluminium in Various Conditions. *Mater. Des.* **2009**, *30*, 3731–3737. [[CrossRef](#)]
21. Kwolek, P.; Obłój, A.; Kościelniak, B.; Buszta, R.; Tokarski, T.; Krupa, K.; Gradzik, A.; Nowak, W.J.; Wojnicki, M.; Motyka, M. Wear Resistance of Hard Anodic Coatings Fabricated on 5005 and 6061 Aluminum Alloys. *Arch. Civ. Mech. Eng.* **2024**, *24*, 51. [[CrossRef](#)]
22. Sheasby, P.G.; Pinner, R.; Wernick, S. *The Surface Treatment and Finishing of Aluminium and Its Alloys*; ASM International: Almere, The Netherlands, 2001.
23. Kim, H.S.; Kim, D.H.; Lee, W.; Cho, S.J.; Hahn, J.H.; Ahn, H.S. Tribological Properties of Nanoporous Anodic Aluminum Oxide Film. *Surf. Coat. Technol.* **2010**, *205*, 1431–1437. [[CrossRef](#)]
24. Lu, J.; Wei, G.; Yu, Y.; Guo, C.; Jiang, L. Aluminum Alloy AA2024 Anodized from the Mixed Acid System with Enhanced Mechanical Properties. *Surf. Interfaces* **2018**, *13*, 46–50. [[CrossRef](#)]
25. Chen, L.; Liu, Z.; Wang, B.; Song, Q.; Wan, Y.; Chen, L. Surface Characterization and Tribological Performance of Anodizing Micro-Textured Aluminum-Silicon Alloys. *Materials* **2019**, *12*, 1862. [[CrossRef](#)] [[PubMed](#)]
26. Soffritti, C.; Fortini, A.; Nastruzzi, A.; Sola, R.; Merlin, M.; Garagnani, G.L. Dry Sliding Behavior of an Aluminum Alloy after Innovative Hard Anodizing Treatments. *Materials* **2021**, *14*, 3281. [[CrossRef](#)] [[PubMed](#)]
27. Santecchia, E.; Cabibbo, M.; Hamouda, A.M.S.; Musharavati, F.; Popelka, A.; Spigarelli, S. Dry Sliding Tribological Properties of a Hard Anodized Aa6082 Aluminum Alloy. *Metals* **2020**, *10*, 207. [[CrossRef](#)]
28. Mohitfar, S.H.; Mahdavi, S.; Etmnanfar, M.; Khalil-Allafi, J. Characteristics and Tribological Behavior of the Hard Anodized 6061-T6 Al Alloy. *J. Alloys Compd.* **2020**, *842*, 155988. [[CrossRef](#)]
29. Tsyntaru, N.; Kavas, B.; Sort, J.; Urgen, M.; Celis, J.P. Mechanical and Frictional Behaviour of Nano-Porous Anodized Aluminium. *Mater. Chem. Phys.* **2014**, *148*, 887–895. [[CrossRef](#)]
30. Benea, L.; Dumitrascu, V. Enhancement in Sustained Friction and Wear Resistance of Nanoporous Aluminum Oxide Films Obtained by Controlled Electrochemical Oxidation Process. *RSC Adv.* **2019**, *9*, 25056–25063. [[CrossRef](#)]
31. Sola, R.; Tonelli, L.; Shashkov, P.; Bogdanoff, T.H.; Martini, C. Anodizing of AA6082-T5 by Conventional and Innovative Treatments: Microstructural Characterization and Dry Sliding Behaviour. *Wear* **2020**, *458–459*, 203423. [[CrossRef](#)]
32. Ikeda, T.; Kinju, T.; Matsuo, Y. Method for Surface Treatment of Aluminum or Aluminum Alloys. EU Patent 1207220B1, 16 January 2008.
33. Liu, S.; Peyronnel, A.; Wang, Q.J.; Keer, L.M. An Extension of the Hertz Theory for 2D Coated Components. *Tribol. Lett.* **2005**, *18*, 505–511. [[CrossRef](#)]
34. van der Zwaag, S.; Field, J.E. The Effect of Thin Hard Coatings on the Hertzian Stress Field. *Philos. Mag. A* **1982**, *46*, 133–150. [[CrossRef](#)]
35. Matthewson, M.J. Axi-Symmetric Contact on Thin Compliant Coatings. *J. Mech. Phys. Solids* **1981**, *29*, 89–113. [[CrossRef](#)]
36. Holmberg, K.; Laukkanen, A.; Ronkainen, H.; Wallin, K.; Varjus, S.; Koskinen, J. Tribological Contact Analysis of a Rigid Ball Sliding on a Hard Coated Surface. *Surf. Coat. Technol.* **2006**, *200*, 3793–3809. [[CrossRef](#)]
37. Ortega-álvarez, R.; Hernández-Sierra, M.T.; Aguilera-Camacho, L.D.; Bravo-Sánchez, M.G.; Moreno, K.J.; García-Miranda, J.S. Tribological Performance of 100Cr6/8620 Steel Bearing System under Green Oil Lubrication. *Metals* **2022**, *12*, 362. [[CrossRef](#)]
38. Dervishi, E.; McBride, M.; Edwards, R.; Gutierrez, M.; Li, N.; Buntyn, R.; Hooks, D.E. Mechanical and Tribological Properties of Anodic Al Coatings as a Function of Anodizing Conditions. *Surf. Coat. Technol.* **2022**, *444*, 128652. [[CrossRef](#)]
39. Methods, A.T. Standard Test Method for Wear Testing with a Pin-on-Disk Apparatus 1. *Wear* **2011**, *5*, 1–5.
40. Ravikiran, A. Influence of Apparent Pressure on Wear Behavior of Self-Mated Alumina. *J. Am. Ceram. Soc.* **2000**, *83*, 1302–1304. [[CrossRef](#)]
41. Kato, K.; Adachi, K. Wear of Advanced Ceramics. *Wear* **2002**, *253*, 1097–1104. [[CrossRef](#)]
42. He, C.C. Preventing Cracking of Anodized Coatings. *NASA Tech. Memo* **1995**, *104622*, 1–13.
43. Wielage, B.; Nickel, D.; Alisch, G.; Podlesak, H.; Lampke, T. Effects of Pre-Treatment on the Growth Rate and Morphology of Hard Anodic Films on Aluminium (EN AW-6082). *Surf. Coat. Technol.* **2007**, *202*, 569–576. [[CrossRef](#)]
44. Baroni, E.; Fortini, A.; Soffritti, C.; Merlin, M.; Garagnani, G.L. Influence of the Nanoporous Alumina Layer Characteristics on the Tribological Behaviour of EN AW-6082 Aluminum Alloy Treated by an Innovative Hard Anodizing Process. *La Metall. Ital.* **2023**, *77*, 41–51.

45. Malayoglu, U.; Tekin, K.C.; Malayoglu, U.; Shrestha, S. An Investigation into the Mechanical and Tribological Properties of Plasma Electrolytic Oxidation and Hard-Anodized Coatings on 6082 Aluminum Alloy. *Mater. Sci. Eng. A* **2011**, *528*, 7451–7460. [[CrossRef](#)]
46. Liu, W.; Zuo, Y.; Tang, Y.; Zhao, X. The Cracking Behavior of Anodic Films on Cast Aluminum Alloy after Heating in the Temperature Range up to 300 °C. *Surf. Coat. Technol.* **2008**, *202*, 4183–4188. [[CrossRef](#)]
47. Ravikiran, A.; Lim, S.C. A Better Approach to Wear-Rate Representation in Non-Conformal Contacts. *Wear* **1999**, 225–229, 1309–1314. [[CrossRef](#)]
48. Ravikiran, A.; Jahanmir, S. Effect of Contact Pressure and Load on Wear of Alumina. *Wear* **2001**, *251*, 980–984. [[CrossRef](#)]
49. Guicciardi, S.; Melandri, C.; Lucchini, F.; de Portu, G. On Data Dispersion in Pin-on-Disk Wear Tests. *Wear* **2002**, *252*, 1001–1006. [[CrossRef](#)]

Disclaimer/Publisher’s Note: The statements, opinions and data contained in all publications are solely those of the individual author(s) and contributor(s) and not of MDPI and/or the editor(s). MDPI and/or the editor(s) disclaim responsibility for any injury to people or property resulting from any ideas, methods, instructions or products referred to in the content.